RESEARCH ARTICLE | OCTOBER 09 2025

Pressure-loss coefficients of Newtonian fluid flows in axisymmetric diffusers

Sergio Rosa ; Adelio Cavadas

Physics of Fluids 37, 103610 (2025)
https://doi.org/10.1063/5.0287386

Physics of Fluids ARTICLE pubs.aip.org/aip/pof

Pressure-loss coefficients of Newtonian fluid flows in axisymmetric diffusers

Cite as: Phys. Fluids **37**, 103610 (2025); doi: 10.1063/5.0287386
Submitted: 24 June 2025 · Accepted: 22 September 2025 ·
Published Online: 9 October 2025

Sergio Rosa[1,a] and Adelio Cavadas[2]

AFFILIATIONS

[1]Polytechnic Institute of Bragança, Campus de Santa Apolónia, 5301-857 Bragança, Portugal
[2]Polytechnic Institute of Viana do Castelo, Avenida do Atlântico, 644, 4900-348 Viana do Castelo, Portugal

[a]**Author to whom correspondence should be addressed:** srosa@ipb.pt. **Tel.:** +351 914107465

ABSTRACT

A comprehensive numerical investigation was conducted on the flow of Newtonian fluids in axisymmetric diffusers across laminar, transitional, and turbulent regimes to quantify the pressure-loss coefficient as a function of Reynolds number, diffuser angle, and diameter expansion ratio. Simulations were performed using ANSYS Fluent software for Reynolds numbers ranging from 2 to 4×10^6, diffuser angles varying from 5° to 90°, and expansion ratios of 1.15, 1.5, and 2. The pressure-loss results are systematically presented in graphics and tables, offering detailed insight into the influence of geometric and flow characteristics on axisymmetric diffuser pressure drop. The complete dataset and a Python interpolation tool are provided as supplementary material to facilitate direct application in engineering analysis.

NOMENCLATURE

C_I	Irreversible pressure-loss coefficient
D_1, D_2	Diameter of inlet and outlet pipes, respectively (m)
REx	Richardson's extrapolated value
f	Darcy friction factor
L	Length (m)
p_2, p_1	Pressure at inlet and outlet planes, respectively (Pa)
Re	Reynolds number
V_1, V_2	Bulk velocity in the inlet and outlet pipes, respectively (m/s)
θ	Diffuser angle (degrees)
ρ	Fluid density (kg/m^3)
σ	Area ratio ($A_1/A_2 = D_1^2/D_2^2$)
ε_{rel}	Relative error (%)
ER	Expansion ratio (D_2/D_1)

I. INTRODUCTION

Piping systems are used in a wide range of industrial applications, used to transport fluids for energy transfer, material processing, and product delivery. Accurate estimation of pumping power in these systems requires detailed knowledge of both frictional and local pressure losses occurring in pipes and fittings. One of the components of such systems is expansion, which can be sudden or gradual, and whose flow behavior has a significant impact on overall system efficiency. Understanding the pressure loss associated with diffusers is therefore essential, particularly as it relates to the flow regime, geometric configuration, and fluid properties. Engineering design calculations often require the estimation of pressure drop, pipe velocity, or pipe diameter, all of which depend critically on accurate values of the local loss coefficient.

Classical fluid dynamics textbooks and empirical references, including Runstadler *et al.* (1975), Crane Co. (2022), Gibson (1930), Idelchik (2005), Massey (1989), Tsui and Wang (1995), and Munson *et al.* (2013), all provide standard correlations for the loss coefficient in diffusers. These expressions are typically derived under simplifying assumptions such as a uniform inlet velocity profile, negligible shear stresses, and rapid flow reattachment. Such correlations generally agree well with experimental data in the turbulent regime; however they fail to capture laminar flow behaior, where shera stresss and viscous effects cannot be neglected. While these expressions remain suitable for turbulent flows, particularly those involving low-viscosity fluids such as air or water, they become increasingly unreliable in laminar regimes where viscous forces play a more dominant role (White, 2006; Fox *et al.*, 2011).

Several researchers have attempted to refine these classical correlations through experimental and numerical approaches. Aziz and El-Shaarawi (1983) conducted experimental studies on pressure losses in diffusers under turbulent conditions, while Suryanarayana and Rao (1994) investigated the influence of inlet velocity profiles. In the context of laminar flow, Oliveira and Pinho (1997) carried out a

numerical investigation of axisymmetric sudden expansions, emphasizing the deviations from classical expressions due to the persistence of shear layers and slower flow redevelopment. Rosa and Pinho (2006) later extended this analysis to include gradual diffusers, again highlighting the inadequacy of traditional loss coefficient formulas for low Reynolds number flows. They found large discrepancies between their local loss coefficient and expressions from the literature, which were based on fast flow redevelopment and negligible shear flow at low Reynolds numbers.

Applications involving high-viscosity fluids and/or small characteristic dimensions, such as polymer extrusion, glass melting, and microfluidic mixing, often operate in the laminar regime (Bird *et al.*, 2007; Tanner, 2000). In such cases, understanding the local pressure losses in expansions is particularly important. Despite this, the literature remains sparse in the transitional regime, which is characterized by complex flow structures and sensitivity to both geometry and inlet conditions (Escudier *et al.*, 2009; Durst *et al.*, 1993). Most available data and correlations are either limited to very low Reynolds numbers or assume fully developed turbulence, resulting in a significant knowledge gap for intermediate conditions with little quantitative information available to guide design.

The present study aims to address these gaps by providing a unified and systematic numerical characterization of the irreversible pressure-loss coefficient (C_I) across laminar, transitional, and turbulent regimes for Newtonian fluid flows through axisymmetric diffusers. Simulations were performed using ANSYS Fluent for Reynolds numbers (Re) ranging from 2 to 4×10^6, covering diffuser angles (θ) from 5° to 90°, and expansion ratios (D_2/D_1) of 1.15, 1.5, and 2.

A study published by Zeng *et al.* (2021) has highlighted how diffuser geometry affects pressure fluctuations and pressure loss in centrifugal systems. Similarly, Shuiguang (2020) investigated internal losses via diffuser optimization in pumps, reinforcing the relevance of geometry and flow condition to diffuser efficiency. Additionally, the findings of Gooding *et al.* (2020) on unsteady pressure effects provide supporting evidence for the consistency between numerical and experimental results related to geometry dependency on pressure losses. These studies highlight the growing emphasis on diffuser performance as governed by geometric configuration and flow regime; however, most focus on either specific design scenarios or restricted flow ranges. In contrast, the present investigation provides a systematic and comprehensive characterization of C_I across laminar, transitional, and turbulent conditions, while spanning a broad range of diffuser angles. This breadth of coverage enables our work to bridge existing gaps and contribute to a robust reference dataset that extends beyond the scope of prior studies.

Advances in Physics of Fluids have revealed novel scaling laws in complex flow regimes, such as curved-duct turbulence (Ali and Dey, 2024) and compressible shock–turbulence interaction (Gao *et al.*, 2023), highlighting the importance of precise physical modeling under transitional or high Reynolds conditions.

Recent studies have demonstrated that hybrid RANS–LES (Reynolds-Averaged Navier-Stokes with Large Eddy Simulation) approaches, sometimes augmented with machine learning-based wall functions, outperform traditional turbulence models in predicting separation and transition in diffuser-like flows (Han, 2024; Davidson, 2025). Concurrently, industry-driven computational fluid dynamics (CFD) optimization of diffuser geometry, using genetic algorithms or neural networks, has produced enhanced diffuser designs tailored for precise pressure recovery (Hwang *et al.*, 2024; Teklemariyem, 2024). In contrast to these works which focus on specific design scenarios or advanced turbulence closures, the current study provides a broad and validated dataset of C_I spanning laminar, transitional, and turbulent regimes across varied angles and expansion ratios, thereby providing a generalizable foundation for both design and modeling in axisymmetric diffuser flows.

The novel contributions of this work are as follows:

1- It provides a comprehensive dataset of C_I values over an extended range of geometric and flow parameters not previously published.
2- It identifies and quantifies the regime in which C_I becomes nearly independent of both Reynolds number and geometry, revealing a previously undocumented plateau in the transitional regime.
3- It validates numerical results against analytical solutions and literature benchmarks for both laminar and turbulent flows, ensuring methodological robustness.
4- It complements and extends existing knowledge, offering a more comprehensive predictive framework for diffuser flow applications.

These findings are directly applicable to the design and optimization of fluid transport systems and provide a solid reference for benchmarking future computational and experimental studies of axisymmetric diffusers.

Some industrial fluids exhibit complex rheological behavior that cannot be adequately described by the Newtonian constitutive equations. In such cases, non-Newtonian models are required to capture the flow dynamics accurately. However, the present study focuses exclusively on Newtonian fluids, as several fundamental aspects of laminar flow through gradually expanding geometries remain insufficiently understood. A comprehensive understanding of Newtonian behavior in these configurations is essential as a foundation for future investigations into more complex, non-Newtonian flows.

The following section introduces the problem definition and outlines the key dimensionless parameters involved in this investigation. This is followed by a detailed description of the numerical methods used to solve the governing equations. Subsequently, an assessment of numerical uncertainty is provided, along with a validation and verification of the results through comparison with existing data from the literature. The final sections present the numerical findings, discuss their implications, and conclude with a summary of the main insights derived from this study.

II. PROBLEM FORMULATION AND GOVERNING PARAMETERS

A schematic representation of the control volumes used in the study is shown in Fig. 1, which illustrates the flow through an axisymmetric gradual expansion. The inlet section is positioned sufficiently far upstream of the diffuser to ensure that fully developed flow conditions are established prior to the onset of the geometric expansion, thereby allowing the flow to respond more realistically to the change in cross section.

In engineering practice, pressure drop calculations in straight pipes are typically based on the assumption of fully developed flow, with all other effects, such as flow distortions and flow redevelopment downstream of fittings, introduced via their respective local loss coefficients. The effects of geometrical disturbances, such as expansions, contractions, or other fittings, are accounted for using empirical or numerical local loss coefficients.

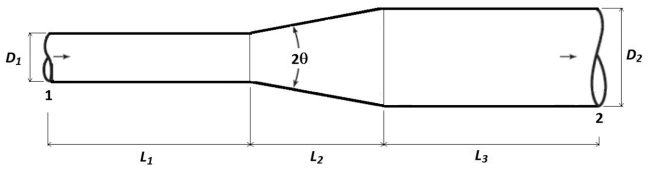

FIG. 1. Gradual expansion geometry with inlet and outlet pipes. The inlet pipe has diameter D_1 and length L_1, the outlet pipe has diameter D_2 and length L_3, and the gradual expansion section has length L_2 and diffuser half-angle θ. Flow enters from the left (plane 1) with a uniform velocity profile, develops fully in the inlet pipe, expands in the diffuser, and exits through the outlet pipe (plane 2) after pressure recovery.

The total pressure change between two cross-sectional planes, denoted as planes 1 and 2 in Fig. 1, can be decomposed into three components: (i) a reversible pressure change due to cross-sectional area variation, (ii) an irreversible pressure drop due to energy dissipation, and (iii) frictional losses in the upstream and downstream pipes.

Accurate evaluation of the irreversible pressure-loss coefficient (C_I) must account for frictional contributions, as the actual frictional effect between planes 1 and 2 differs from that predicted by the assumption of fully developed flow alone. In this study, C_I is determined from the axial pressure distribution obtained via the numerical solution of the full Navier–Stokes equations, allowing the dissipation and frictional deviations from ideal flow to be quantified accurately.

The energy equation applied between cross sections 1 and 2 (see Fig. 1) for a fully developed, incompressible, and steady-state flow, can be written as

$$p_1 + \frac{1}{2}\rho V_1^2 + \rho g Z_1 = p_2 + \frac{1}{2}\rho V_2^2 + \rho g Z_2 + f_1 \frac{L_1}{D_1}\rho \frac{V_1^2}{2} + f_2 \frac{L_3}{D_2}\rho \frac{V_2^2}{2} + \frac{1}{2}\rho V_1^2 C_I, \tag{1}$$

where p is the static pressure, ρ is the fluid density, V is the bulk velocity, Z is the elevation, f the Darcy friction factor, L the length, D the diameter of the pipe section, and C_I is the irreversible pressure-loss coefficient associated with the diffuser.

Assuming horizontal flow ($Z_1 = Z_2$), applying mass conservation ($A_1 V_1 = A_2 V_2$), and defining the area ratio as $\sigma = A_1/A_2$, the equation can be rearranged and simplified, so the expression for the irreversible pressure-loss coefficient becomes

$$C_I = \frac{p_1 - p_2}{\frac{1}{2}\rho V_1^2} - f_1 \frac{L_1}{D_1} - f_2 \frac{L_3}{D_2}\sigma^2 + (1 - \sigma^2). \tag{2}$$

The Darcy friction factors f_1 and f_2, for the inlet and outlet pipes respectively, are determined based on the flow regime as

$$\begin{cases} f = \dfrac{64}{Re}, & \text{Laminar (Hagen} - \text{Poiseuille law)}, \\ \dfrac{1}{\sqrt{f}} = 2\,log\left(Re f^{\frac{1}{2}}\right) - 0,8, & \text{Turbulent (Prandtl} - \text{Karman law)}. \end{cases} \tag{3}$$

These equations are presented in classical fluid mechanics references such as White (2022) and Shames (1992), and they ensure accurate evaluation of frictional losses in both laminar and turbulent regimes in straight pipes.

The static pressures at stations 1 and 2 (p_1 and p_2) were obtained from the numerical solution of the full Navier–Stokes equations, performed using the commercial computational fluid dynamics (CFD) ANSYS Fluent software.

III. NUMERICAL PROCEDURE, UNCERTAINTIES, AND VALIDATION

In many practical engineering applications, it is not possible to obtain exact analytical solutions due to the inherent complexity of the governing differential equations or the challenges posed by intricate boundary and initial conditions. Analytical solutions, when available, provide continuous and exact descriptions of system behavior throughout the domain. However, numerical methods offer an alternative by approximating the solution at discrete points, known as nodes, which are distributed throughout the domain. This discretization process is a fundamental step in any numerical procedure and involves subdividing the physical domain into a finite number of smaller subregions or elements.

Three main numerical methods are used to solve partial differential equations in engineering and physics: finite difference method (FDM), finite element method (FEM), and finite volume method (FVM). With FDM, the differential equation is written for each node, and the derivatives are replaced by difference equations. This approach results in a set of simultaneous linear equations. Although finite difference methods are easy to understand and employ in simple problems, they are become difficult to apply in problems with complex geometry or complex boundary conditions; this situation is also true for problems with non-isotropic material properties. The FEM, by contrast, uses integral formulations rather than difference equations to create a system of algebraic equations. Moreover, an approximate continuous function is assumed to represent the solution for each element. The complete solution is then generated by connecting or assembling the individual solutions, allowing for continuity at the inter-elemental boundaries. The FVM is based on the application of conservation laws to control volumes that subdivide the computational domain. The governing equations are integrated over each control volume, and fluxes of conserved quantities (such as mass, momentum, or energy) are computed across the control volume faces. This method ensures local and global conservation, which is a key advantage in fluid dynamics and heat transfer applications. FVM handles both structured and unstructured grids well, making it highly suitable for solving complex flow problems with arbitrary geometries. It is the foundational method in most commercial CFD solvers, such as ANSYS Fluent.

ANSYS Fluent provides a robust and versatile platform for solving the full Navier–Stokes equations under a variety of conditions. In the study, ANSYS Fluent was employed to perform detailed numerical simulations of fluid flow through axisymmetric diffusers, enabling the evaluation of irreversible pressure-loss coefficients under various flow regimes and geometric configurations.

The simulations were performed using ANSYS Fluent, a commercial finite-volume based CFD solver, capable of accurately resolving fluid flows across a broad range of Reynolds numbers by solving the full incompressible Navier–Stokes equations in steady state. The pressure-based solver was employed with second-order upwind

schemes for momentum discretization, and a pressure–velocity coupling was achieved using the SIMPLE algorithm.

Simulations were conducted across an extensive range of Reynolds numbers, spanning from the laminar to the fully turbulent regime (from $Re = 2$ to 4×10^6), with the Reynolds number based on the inlet bulk velocity. For laminar flows ($Re < 2000$), the laminar model in Fluent was used. For transitional flows ($Re = 2000$–4000), the simulations were conducted using the Transition SST model, which blends laminar and turbulent modeling by accounting for intermittency and the transition onset criteria based on local Reynolds numbers and turbulence intensity. This approach allowed for a more accurate representation of the flow behavior in the regime where neither purely laminar nor fully turbulent assumptions hold. For turbulent flows ($Re > 4000$), the standard k–ω Shear Stress Transport (SST) model was selected due to its well-documented performance in predicting separation and reattachment flows in diffusers.

A series of preliminary simulations were performed using multiple mesh configurations to evaluate the appropriate size of the computational domain and ensure grid-independent results. These tests also served to determine the necessary lengths of the inlet and the outlet pipes to allow for the full development of the velocity profile. A uniform velocity profile at the inlet was imposed to facilitate realistic flow development well upstream the beginning of the diffuser. In this preliminary stage, the influence of mesh refinement, pipe lengths, and their interaction with the Reynolds number was systematically examined to assess their impact on solution accuracy and the reliability of the numerical results.

The computational domain was meshed using structured, axisymmetric quadrilateral elements, with finer resolution near walls and in regions of high velocity gradients. The inlet pipe had a diameter of 10 cm, with a length corresponding to 50 diameters ($L_1 = 50\,D_1$) to ensure fully developed flow conditions. The length of the outlet pipe was extended to a length of $L_3 = 100\,D_1$ to allow for pressure recovery and flow stabilization.

Boundary conditions included an uniform velocity inlet profile, a zero gradient pressure at the outlet, and no-slip wall conditions were applied throughout. Convergence was ensured by requiring residuals below 10^{-6} for continuity and momentum equations, and less than 1% variation in the monitored pressure-drop coefficient between iterations.

Three diameter expansion ratios (D_2/D_1) were considered in this investigation: 1:1.15, 1:1.5, and 1:2. The selection of these expansion ratios was made with both practical relevance and physical insight in mind. Expansion ratios of 1.5 and 2.0 are among the most commonly encountered in industrial applications, including piping systems, ventilation ducts, and fluid transport components, and are frequently referenced in experimental and numerical studies of diffusers. These values therefore serve as representative cases for engineering practice. The inclusion of a smaller expansion ratio ($D_2/D_1 = 1.15$) was intentional to allow for a more detailed analysis of the evolution of pressure-loss coefficients as a function of geometric expansion. It provides insight into the behavior of flows with minimal divergence and serves as a baseline to understand the transition in flow structure and energy loss characteristics between compact and more aggressive diffusers.

The diffuser length L_2 varied depending on both the expansion ratio D_2/D_1 and the diffuser angle θ, while the number of computational cells within the diffuser was adjusted accordingly to maintain consistent mesh resolution and quality.

To estimate the numerical uncertainty associated with the irreversible pressure-loss coefficient C_I results, mesh refinement studies were conducted for two selected diffuser angle calculations ($\theta = 20°$, $\theta = 60°$), both having the same expansion ratio $D_2/D_1 = 2$. For each configuration, simulations were performed using three successively refined meshes, coarse, medium, and fine, with maximum cell sizes of 10, 5, and 3 mm, respectively.

Tables I and II summarize the mesh refinement study, presenting the calculated C_I values for each of the three meshes, along with the extrapolated reference value obtained using Richardson's deferred approach to the limit (Richardson, 1927). The relative errors (ε_{rel}) were computed with respect to the extrapolated values. The results show that the fine mesh consistently achieved numerical uncertainties below 2%, demonstrating that further refinement would not yield a significant improvement in the accuracy of C_I. All relative errors not exceeding 2% are presented in bold to emphasize the intended message, namely the convergence behavior and the high accuracy of the fine mesh relative to the Richardson extrapolated (REx) values. Accordingly, the fine mesh, comprising approximately 150 000 cells, was selected for all simulations across the full range of diffuser angles, expansion ratios, and flow regimes.

All simulations were performed on a system equipped with an Intel Xeon W-2195 CPU operating at 2.30 GHz, using eight solver processors and double-precision settings in ANSYS Fluent. Each simulation required an average of approximately 240 minutes of CPU time.

To validate the numerical results, two limiting cases with available data in the literature were investigated: (1) fully developed pipe flow, corresponding to the limit case of a diffuser tending toward a straight pipe (i.e., $\theta \to 0$, and $D_2/D_1 \to 1$), and (2) sudden expansion, corresponding to a diffuser with $\theta = 90°$.

For the first case, the equivalent irreversible pressure-loss coefficient C_I was computed for a nearly straight pipe ($\theta = 0.5$) as the expansion ratio D_2/D_1 approached unity. The results, shown in Fig. 2, illustrate the convergence of C_I toward the theoretical predictions for fully developed flow: the Hagen–Poiseuille equation in the laminar regime, and the Prandtl–Karman equation in the turbulent regime [Eq. (3)]. The simulations were conducted using a pipe length of 150 times the inlet diameter for all expansion ratios, ensuring flow development within the fully developed region. As the expansion ratio decreased to $D_2/D_1 = 1$, the calculated values of C_I closely matched the theoretical solutions, confirming the accuracy of the numerical methodology for this limiting case.

For the second validation case, sudden expansion ($\theta = 90°$), the numerical results were compared with reference data from the literature. Figures 3 and 4 present the calculated irreversible pressure-loss coefficient for sudden expansions with diameter ratios $D_2/D_1 = 2$ and $D_2/D_1 = 1.5$, respectively.

In the laminar flow regime, the computed results exhibit a similar trend to those reported by Rosa and Pinho (2006) and Pinho *et al.*, (1998). However, noticeable discrepancies are observed for very low Reynolds numbers. For the case of $D_2/D_1 = 2$, the deviation in C_I increases significantly, from approximately 3% at $Re = 100$ to nearly 60% at $Re = 2$. These differences highlight the inadequacy of traditional loss coefficient formulas when applied to low Reynolds number flows. Here, we also notice these discrepancies between local loss coefficient results and the expressions from the literature, which are based on assumptions that include fast flow redevelopment after expansion

TABLE I. Mesh refinement study for a diffuser with expansion ratio $D_2/D_1 = 2.0$ and diffuser angle $\theta = 60°$. The table reports the irreversible pressure-loss coefficient (C_I) for three mesh densities (coarse, medium, fine) at various Reynolds numbers (Re), together with the Richardson extrapolated (REx) reference value and the corresponding relative error ε_{rel} (%). Values in bold indicate $\varepsilon_{rel} \leq 2\%$, confirming mesh convergence for the fine mesh.

Re	Coarse C_I	ε_{rel} (%)	Medium C_I	ε_{rel} (%)	Fine C_I	ε_{rel} (%)	REx
2	20.268	30	24.768	7	25.794	**2**	26.381
5	8.268	25	10.000	3	10.230	**1**	10.339
10	4.056	45	5.660	4	5.823	**1**	5.887
20	2.588	25	3.056	6	3.167	**2**	3.232
50	1.678	7	1.842	3	1.818	**1**	1.796
100	1.441	**1**	1.500	5	1.457	**2**	1.425
200	1.375	**0**	1.425	4	1.396	**2**	1.374
500	1.337	**0**	1.384	4	1.356	**2**	1.335
1000	1.267	**1**	1.327	4	1.300	**2**	1.279
2000	1.006	**1**	1.051	4	1.030	**2**	1.013
4000	0.777	**1**	0.815	6	0.789	**2**	0.770
8000	0.627	5	0.664	**1**	0.660	**1**	0.655
16 000	0.567	**1**	0.596	4	0.584	**2**	0.575
32 000	0.535	**1**	0.558	4	0.546	**2**	0.538
64 000	0.504	**1**	0.530	4	0.519	**2**	0.511
128 000	0.483	**1**	0.506	4	0.496	**2**	0.488
256 000	0.477	**0**	0.495	4	0.485	**2**	0.477
512 000	0.470	**0**	0.486	4	0.477	**2**	0.469
1 024 000	0.464	**1**	0.478	4	0.469	**2**	0.462
2 048 000	0.4567	**0**	0.473	4	0.464	**2**	0.457
4 096 000	0.452	**1**	0.465	4	0.456	**2**	0.449

and negligible viscous shear dominance over inertial effects. However, at low Reynolds numbers, these assumptions no longer hold: shear stresses and viscous diffusion become the prevailing mechanisms, significantly influencing the development of the velocity profile along the diffuser walls. As a result, the pressure-loss behavior deviates notably from classical models, highlighting the need for more accurate formulations that account for viscous effects in laminar and transitional flow regimes.

For the turbulent flow regime, the computed values of C_I show excellent agreement with the empirical correlation presented in White (2022),

$$C_I = \begin{cases} 2.61 \cdot \sin\theta\,(1-\sigma)^2 & \theta \leq 22.5°, \\ (1-\sigma)^2 & 22.5° < \theta \leq 90°. \end{cases} \tag{4}$$

This correlation [Eq. (4)], widely adopted in engineering practice, is based on experimental data and theoretical considerations for turbulent flows through sudden expansions. The close match between the present numerical results and the established correlation further validates the accuracy and robustness of the simulation methodology for high Reynolds number flows.

Figures 3 and 4 also illustrate the evolution of C_I as the diffuser angle (θ) increases from 60° to 90°. The results clearly show that, for $\theta = 80°$, the values of C_I are already very close to those observed for a sudden expansion ($\theta = 90°$). This indicates that beyond a certain angular threshold, approximately 80°, the flow behavior and associated pressure losses approach those characteristic of an sudden expansion, with minimal additional impact from further increasing of the expansion angle. This explains why C_I results deviate from the reference data [Eq. (4)] when the expansion angle decreases further, as well observed for $\theta = 60°$.

IV. RESULTS

The variation of C_I with Reynolds number (Re) and diffuser angle (θ) for Newtonian fluids is presented in Figs. 5–7, for expansion ratios $D_2/D_1 = 2$, $D_2/D_1 = 1.5$, and $D_2/D_1 = 1.15$, respectively. Both diffuser geometry and flow regime exert a strong influence on C_I.

In the laminar regime, for a fixed Re, C_I decreases as θ increases, as it happens in the turbulent regime, where C_I also decreases with increasing θ, although the rate of variation differs. At a constant diffuser angle, C_I decreases with increasing Re, highlighting the relation between viscous and inertial forces in determining flow behavior. At low Reynold numbers, where viscous forces predominate, the pressure variation scales with viscous stress, leading to a C_I varying linearly with $1/Re$. For example, for $\theta = 5°$ and $D_2/D_1 = 2$, C_I increases by a factor of 46, from 1.890 to 86.246, as Re decreases from 100 to 2.

In contrast, at high Reynolds numbers, where inertial forces dominate, the pressure variation scales with kinetic energy, and C_I asymptotically approaches a constant value. For example, in the same geometry ($\theta = 5°$ and $D_2/D_1 = 2$), increasing Re from 128 000 to 2 048 000 yields only a modest decrease in C_I by a factor of 1.6 (from 0.131 to 0.084).

The sensitivity of C_I to diffuser angle is especially pronounced at low Re. For example, at $Re = 5$ and $D_2/D_1 = 2$, the value of C_I at $\theta = 5°$

TABLE II. Mesh refinement study for a diffuser with expansion ratio $D_2/D_1 = 2.0$ and angle $\theta = 20°$. As in Table I, the irreversible pressure-loss coefficient (C_I) is shown for coarse, medium, and fine meshes at multiple Reynolds numbers (Re), with the Richardson extrapolated (REx) value and the relative error ε_{rel} (%). Bold values highlight relative errors $\leq 2\%$, demonstrating that the fine mesh resolution is sufficient for accurate C_I prediction.

Re	Coarse C_I	ε_{rel} (%)	Medium C_I	ε_{rel} (%)	Fine C_I	ε_{rel} (%)	REx
2	28.724	24	33.238	7	34.646	**2**	35.506
5	11.618	23	13.406	7	13.960	**2**	14 298
10	5.979	22	6.869	6	7.133	**2**	7.292
20	3.277	19	3.724	5	3.839	**2**	3.907
50	1.861	3	1.928	**0**	1.928	**0**	1.926
100	1.441	3	1.484	**0**	1.484	**0**	1.483
200	1.398	4	1.450	**0**	1.451	**0**	1.450
500	1.411	**1**	1.463	4	1.429	**2**	1.403
1000	1.325	**1**	1.396	4	1.363	**2**	1.336
2000	1.041	**1**	1.079	4	1.053	**2**	1.033
4000	0.733	5	0.768	**0**	0.768	**0**	0.767
8000	0.546	6	0.578	**0**	0.578	**0**	0.577
16 000	0.428	5	0.448	**0**	0.448	**0**	0.448
32 000	0.365	6	0.388	**0**	0.387	**0**	0.387
64 000	0.338	5	0.356	**0**	0.356	**0**	0.355
128 000	0.314	3	0.325	**0**	0.325	**0**	0.325
256 000	0.289	**2**	0.295	**0**	0.295	**0**	0.295
512 000	0.264	**2**	0.271	**0**	0.271	**0**	0.270
1 024 000	0.245	3	0.252	**0**	0.252	**0**	0.252
2 048 000	0.230	3	0.238	**0**	0.238	**0**	0.237
4 096 000	0.213	5	0.223	**0**	0.223	**0**	0.223

is approximately 3.6 times greater than at $\theta = 90°$. However, at higher Reynolds numbers but still within the laminar regime, this sensitivity diminishes. For example, at Re =500, C_I varies by only 10% when θ increases from 5° to 90°.

These trends of C_I with θ, in the laminar region, may appear in contradiction with conventional design principles according to which smaller diffuser angles improve flow efficiency. However, C_I accounts for all sources of flow perturbations, which occur over different lengths

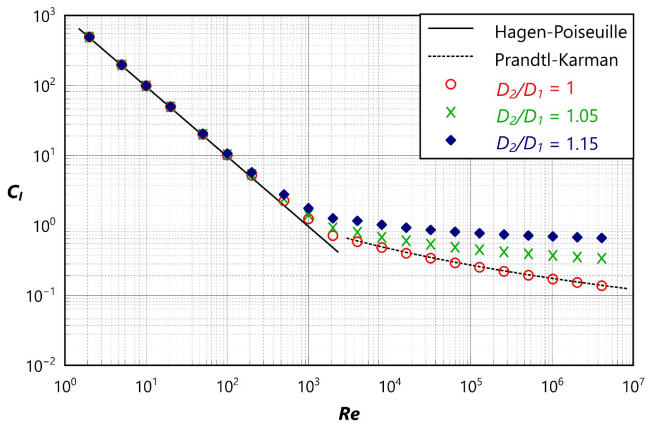

FIG. 2. Validation of the numerical approach for the limiting case of fully developed pipe flow. The irreversible pressure-loss coefficient (C_I) is shown as a function of Reynolds number (Re) for a small expansion angle ($\theta = 0.5°$) as the expansion ratio D_2/D_1 tends to1. Numerical results converge to the theoretical predictions for laminar flow (Hagen–Poiseuille equation) and turbulent flow (Prandtl–Karman equation), confirming solver accuracy to the limit case of a diffuser tending toward a straight pipe.

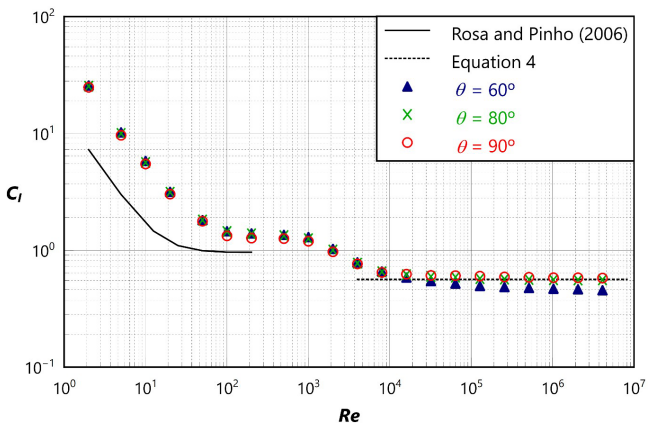

FIG. 3. Calculated irreversible pressure-loss coefficient (C_I) vs Reynold number (Re) for high diffuser angles ($\theta = 90°$, 80°, and 60°) with expansion ratio $D_2/D_1 = 2$. Numerical results are compared with the laminar regime correlation of Rosa and Pinho (2006) and the turbulent regime correlation given by Eq. (4). The plot illustrates that for $\theta = 80°$, C_I values are already close to those for a sudden expansion, indicating minimal additional pressure loss when increasing the angle further.

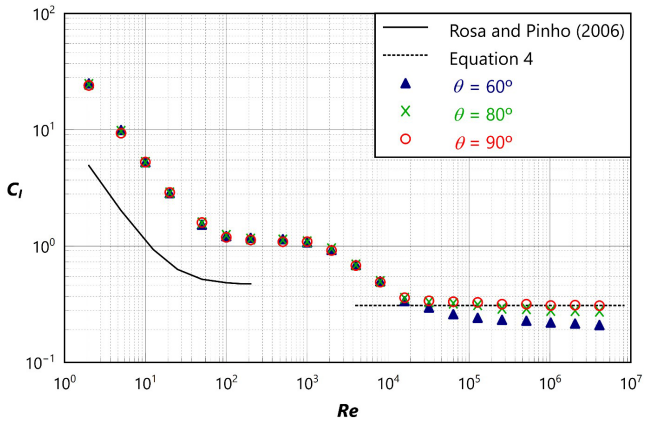

FIG. 4. Calculated irreversible pressure-loss coefficient (C_I) vs Reynold number (Re) for high diffuser angles ($\theta = 90°$, 80°, and 60°) with expansion ratio $D_2/D_1 = 1.5$. Numerical results are compared with the laminar regime correlation of Rosa and Pinho (2006) and the turbulent regime correlation given by Eq. (4). As in Fig. 3, the results show that beyond $\theta \approx 80°$, the flow behavior approaches that of a sudden expansion, with negligible impact on C_I from further angle increases.

of pipe for different diffuser angles. As the diffuser angle θ increases, the diffuser length L_2 decreases; consequently, the frictional pressure losses within the diffuser decrease, reaching zero for a sudden expansion. In contrast, the irreversible losses due to inefficient flow deceleration and enhanced velocity and pressure distortions increase significantly with θ, explaining the observed variations in C_I.

In the turbulent regime, the trend aligns with classical expectations: C_I decreases significantly with decreasing diffuser angle. For example, at $Re = 4\,096\,000$ and $D_2/D_1 = 2$, C_I at $\theta = 90°$ is 7.6 times greater than at $\theta = 5°$. This confirms that, in turbulent flows, diffusers with smaller expansion angles are markedly more efficient than those with abrupt or large expansion angles.

Another noteworthy conclusion is that, as the Reynolds number increases from the laminar to the transitional regime, between laminar and turbulent flow, the irreversible pressure-loss coefficient C_I tends to

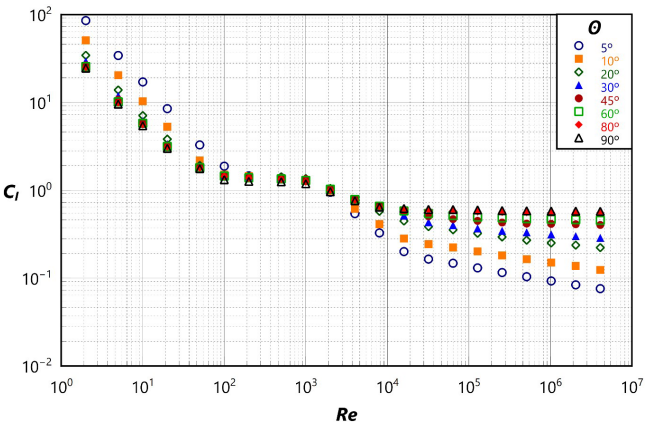

FIG. 5. Calculated irreversible pressure-loss coefficient (C_I) as function of Reynolds number (Re) and diffuser angle (θ), for expansion ratio $D_2/D_1 = 2$. Results highlight C_I trends across laminar, transitional, and turbulent regimes.

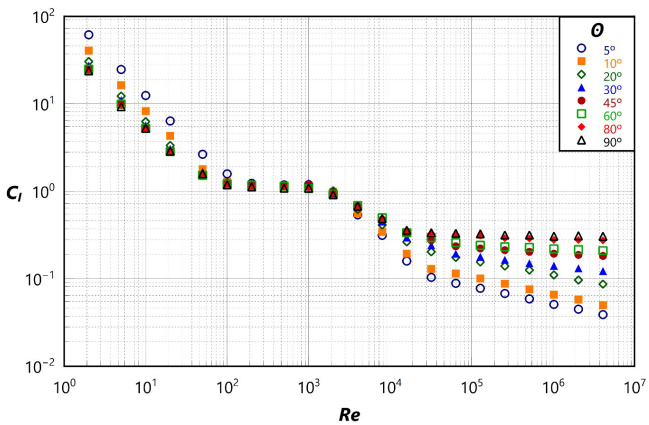

FIG. 6. Calculated irreversible pressure-loss coefficient (C_I) as function of Reynolds number (Re) and diffuser angle (θ), for expansion ratio $D_2/D_1 = 1.5$.

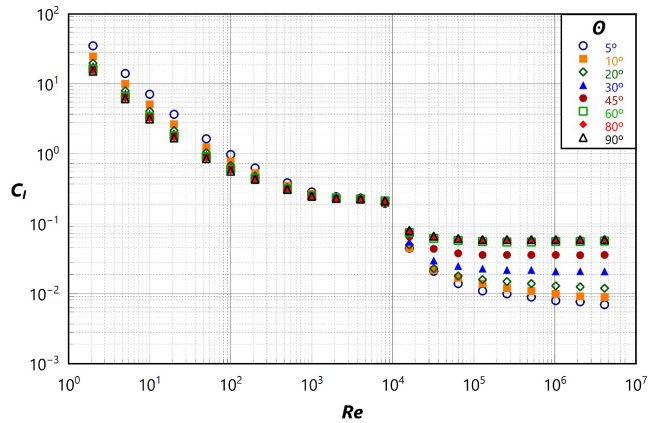

FIG. 7. Calculated irreversible pressure-loss coefficient (C_I) as function of Reynolds number (Re) and diffuser angle (θ), for expansion ratio $D_2/D_1 = 1.15$.

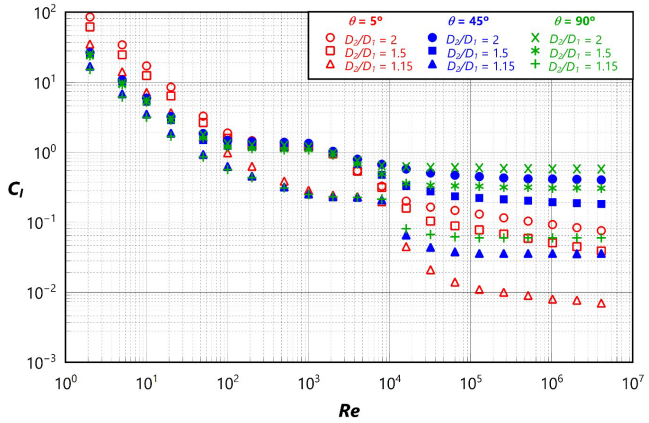

FIG. 8. Evolution of the calculated irreversible pressure-loss coefficient (C_I), as function of Reynolds number (Re), for the diameter expansion ratios studied ($D_2/D_1 = 1.15$, 1.5, and 2), at selected diffuser angles ($\theta = 5°$, $\theta = 45°$, $\theta = 90°$). The combined plot facilitates direct evaluation of the influence of expansion ratio on pressure-loss performance across flow regimes.

TABLE III. Calculated irreversible pressure-loss coefficient (C_l), for different Reynolds numbers (Re), spanning from laminar to turbulent regimes, eight diffuser angles ($\theta = 5°$–$90°$), and three expansion ratios ($D_2/D_1 = 2$, $D_2/D_1 = 1.5$, $D_2/D_1 = 1.15$).

$D_2/D_1 = 2$								
Re / θ	5°	10°	20°	30°	45°	60°	80°	90°
2	86.246	51.299	34.646	29.564	26.688	25.794	25.329	24.795
5	34.480	20.569	13.960	11.956	10.823	10.230	9.976	9.630
10	17.244	10.367	7.133	6.177	5.964	5.823	5.629	5.472
20	8.556	5.326	3.839	3.371	3.257	3.167	3.133	3.019
50	3.300	2.198	1.928	1.899	1.861	1.818	1.811	1.772
100	1.890	1.519	1.484	1.484	1.485	1.457	1.445	1.327
200	1.468	1.461	1.451	1.440	1.426	1.396	1.382	1.269
500	1.393	1.384	1.429	1.407	1.395	1.356	1.334	1.257
1000	1.299	1.295	1.363	1.355	1.347	1.300	1.255	1.194
2000	0.953	0.995	1.053	1.056	1.036	1.030	1.004	0.969
4000	0.544	0.618	0.768	0.794	0.799	0.789	0.774	0.763
8000	0.328	0.413	0.578	0.656	0.675	0.660	0.654	0.645
16 000	0.201	0.283	0.448	0.518	0.578	0.584	0.618	0.623
32 000	0.165	0.244	0.387	0.434	0.508	0.546	0.595	0.608
64 000	0.148	0.224	0.356	0.401	0.471	0.519	0.588	0.606
128 000	0.131	0.202	0.325	0.369	0.450	0.496	0.572	0.600
256 000	0.116	0.182	0.295	0.346	0.431	0.485	0.566	0.590
512 000	0.104	0.165	0.271	0.333	0.419	0.477	0.562	0.586
1 024 000	0.093	0.151	0.252	0.315	0.416	0.469	0.558	0.581
2 048 000	0.084	0.138	0.238	0.301	0.412	0.464	0.557	0.581
4 096 000	0.076	0.124	0.223	0.288	0.404	0.456	0.558	0.578

$D_2/D_1 = 1.5$								
Re / θ	5°	10°	20°	30°	45°	60°	80°	90°
2	62.123	40.909	30.684	27.534	25.574	25.122	24.562	24.058
5	24.911	16.441	12.361	11.107	10.337	9.977	9.700	9.350
10	12.545	8.324	6.307	5.696	5.323	5.280	5.250	5.280
20	6.409	4.329	3.359	3.073	2.903	2.861	2.870	2.894
50	2.666	1.800	1.575	1.670	1.498	1.533	1.586	1.595
100	1.591	1.290	1.275	1.271	1.238	1.221	1.238	1.190
200	1.240	1.200	1.193	1.210	1.200	1.180	1.150	1.130
500	1.190	1.150	1.180	1.190	1.190	1.150	1.129	1.090
1000	1.199	1.140	1.175	1.250	1.200	1.080	1.090	1.091
2000	0.950	0.990	1.018	1.000	0.973	0.930	0.950	0.917
4000	0.540	0.563	0.623	0.661	0.683	0.690	0.689	0.680
8000	0.315	0.345	0.414	0.452	0.477	0.500	0.496	0.490
16 000	0.160	0.194	0.265	0.297	0.330	0.338	0.356	0.360
32 000	0.104	0.130	0.204	0.242	0.276	0.297	0.331	0.338
64 000	0.089	0.115	0.176	0.194	0.236	0.260	0.322	0.332
128 000	0.078	0.101	0.156	0.179	0.223	0.242	0.313	0.328
256 000	0.068	0.088	0.140	0.165	0.213	0.233	0.292	0.317
512 000	0.059	0.076	0.126	0.151	0.204	0.229	0.289	0.317
1 024 000	0.051	0.066	0.111	0.141	0.194	0.220	0.279	0.308
2 048 000	0.045	0.058	0.097	0.132	0.188	0.216	0.278	0.311
4 096 000	0.039	0.050	0.087	0.123	0.183	0.210	0.275	0.307

Table III (*Continued.*)

$D_2/D_1 = 1.15$								
Re / θ	5°	10°	20°	30°	45°	60°	80°	90°
2	35.354	25.010	19.915	18.228	17.072	16.457	15.658	15.300
5	14.199	10.072	8.032	7.357	6.896	6.611	6.325	6.182
10	7.179	5.115	4.101	3.764	3.534	3.416	3.246	3.174
20	3.701	2.674	2.169	2.001	1.888	1.826	1.740	1.704
50	1.653	1.247	1.048	0.977	0.937	0.912	0.877	0.862
100	0.984	0.783	0.685	0.653	0.630	0.608	0.582	0.569
200	0.632	0.533	0.485	0.469	0.458	0.452	0.440	0.435
500	0.388	0.350	0.331	0.325	0.321	0.319	0.313	0.311
1000	0.287	0.268	0.259	0.257	0.255	0.254	0.251	0.249
2000	0.245	0.242	0.238	0.236	0.233	0.232	0.232	0.232
4000	0.234	0.232	0.231	0.230	0.229	0.227	0.227	0.227
8000	0.197	0.198	0.201	0.204	0.210	0.213	0.215	0.215
16 000	0.045	0.045	0.050	0.056	0.066	0.075	0.080	0.081
32 000	0.021	0.022	0.023	0.030	0.044	0.062	0.065	0.067
64 000	0.014	0.017	0.018	0.025	0.038	0.058	0.061	0.062
128 000	0.011	0.014	0.016	0.023	0.036	0.056	0.058	0.061
256 000	0.010	0.012	0.015	0.022	0.036	0.055	0.059	0.060
512 000	0.009	0.011	0.014	0.022	0.036	0.055	0.059	0.060
1 024 000	0.008	0.010	0.013	0.021	0.036	0.056	0.058	0.060
2 048 000	0.008	0.009	0.013	0.021	0.036	0.056	0.059	0.060
4 096 000	0.007	0.009	0.012	0.021	0.036	0.057	0.059	0.060

remain nearly constant. In this intermediate regime, C_I becomes largely independent of both the Reynolds number and the diffuser angle. This suggests a balance between viscous and inertial effects in the transitional flow regime, resulting in a relatively stable dissipation behavior across different geometric and flow conditions. Unlike fully laminar flows, where viscous diffusion dominates, or fully turbulent flows, where inertial forces and turbulent mixing dominate and control pressure losses, transitional flows exhibit mixed characteristics. In the transitional regime, flow separation may be intermittent, reattachment is often delayed, and turbulence production is not yet fully developed across the diffuser. As a result, C_I becomes relatively insensitive to moderate changes in Reynolds number and/or diffuser geometry. This flow behavior produces a range of Reynolds numbers where the energy dissipation mechanisms stabilize, leading to the plateau observed in Figs. 5–7. Such behavior has not been clearly captured in previous experimental or empirical studies, making this a novel contribution.

From an engineering perspective, identifying the plateau in the transitional flow regime carries important practical implications. This is especially relevant for systems such as pumps, ventilation ducts, and flow conditioners, where operating conditions often lie within this regime. In such cases, relying on traditional empirical correlations can result in underestimation or overestimation of pressure losses. The observed near-constant behavior of C_I suggests that once transition begins, moderate changes in Reynolds number or diffuser geometry have limited impact on performance. This understanding supports the design of more compact and efficient diffusers, allowing for improved robustness and predictability in pressure recovery across varying flow conditions.

The variation of C_I for the three diameter expansion ratios investigated is presented in Fig. 8. The results show that C_I is consistently higher for the largest expansion ratio ($D_2/D_1 = 2$). As expected, C_I decreases with decreasing expansion ratio, and this effect is particularly pronounced at the extremes of the flow regime, very low and very high Reynolds numbers. Additionally, Fig. 8 illustrates that, as the Reynolds number increases from the laminar through the transitional regime, and into the turbulent regime, C_I tends to approach a constant value for high Reynolds numbers, especially for lower diffuser angles. This behavior highlights the reduced sensitivity of C_I to flow conditions in the turbulent regime, where inertial forces dominate and diffuser geometry becomes the primary influence on loss characteristics.

Table III lists all the calculated values of the irreversible pressure coefficient as a function of the Reynolds number and the diffuser angle, which constitutes the main outcome of this research work. Table III presents the complete set of calculated values for the irreversible pressure-loss coefficient C_I as a function of the Reynolds number *Re* and the diffuser angle θ. These results represent the main outcome of this research and provide a comprehensive reference for pressure-loss characterization in axisymmetric diffusers across a large range of flow regimes.

To enhance practical usability, a Python script that interpolates the pressure-loss coefficient from Table III is provided. The dataset from Table III and a Python interpolation script are provided in the

supplementary material to enable direct calculation of C_I within the studied parameter ranges.

V. CONCLUSIONS

This study presents a comprehensive numerical investigation of the irreversible pressure-loss coefficient C_I for Newtonian fluid flow through axisymmetric diffusers, spanning a wide range of Reynolds numbers (Re =2 to 4×10^6), diffuser angles ($\theta = 5^\circ$ to 90°), and expansion ratios ($D_2/D_1 = 1.15$, 1.5, and 2).

The results confirm that C_I is primarily governed by the diffuser angle, expansion ratio, and Reynolds number. Large deviations from classical empirical correlations, especially under laminar flow conditions, underscore the limitations of traditional formulas that neglect viscous effects and extended flow redevelopment at low Reynolds numbers.

In the transitional regime, a key finding is the emergence of a plateau behavior, where C_I becomes nearly invariant with respect to both geometric and flow parameters. This phenomenon, not previously documented, suggests a degree of universality not captured by existing models.

In fully turbulent flows, C_I stabilizes progressively as Re increases, indicating a shift toward inertial-dominated behavior. In the limiting case of sudden expansion ($\theta = 90^\circ$), numerical results align well with established empirical expressions, providing validation for the modeling approach. The results also reaffirm that low-angle diffusers minimize pressure losses in turbulent regimes, supporting their use in engineering systems where pressure recovery is critical.

The complete dataset of C_I values (Table III) provides an extensive reference for engineering design. To enhance practical usability, a Python interpolation tool and the complete dataset are provided in the supplementary material to support direct application of these results in engineering design and analysis.

In addition to delivering a large and consistent dataset, this study offers novel insights into the transitional flow regime, expands available pressure-loss data for underexplored Reynolds number ranges, and provides validated modeling results relevant to CFD practitioners and fluid system designers. These outcomes also provide a foundation for future work on non-Newtonian flows and diffuser optimization. The present results offer insight into expected flow behavior, guide mesh and solver configurations, and help identify high shear stress regions where non-Newtonian effects are likely to be significant. Incorporating rheological models will necessitate careful specification of viscosity parameters and flow behavior indices to accurately capture shear-dependent viscosity. Future research can build on these data to validate and enhance non-Newtonian flow predictions under comparable geometrical conditions.

SUPPLEMENTARY MATERIAL

See the supplementary material for (ZIP folder) contains the complete dataset from Table III and a Python interpolation tool, together with detailed usage instructions and example commands, enabling direct calculation of the irreversible pressure-loss coefficient (C_I) for any combination of Reynolds number, diffuser angle, and expansion ratio within the studied parameter ranges.

AUTHOR DECLARATIONS

Conflict of Interest

The authors have no conflicts to disclose.

Author Contributions

Sergio Rosa: Conceptualization (lead); Data curation (lead); Formal analysis (lead); Investigation (lead); Methodology (lead); Supervision (lead); Validation (lead); Visualization (lead); Writing – original draft (lead); Writing – review & editing (lead). **Adélio Cavadas:** Data curation (equal); Visualization (equal); Writing – review & editing (equal).

DATA AVAILABILITY

The data that support the findings of this study are available within the article.

REFERENCES

Ali, S. Z. and Dey, S., "Universal skin friction laws for turbulent flow in curved tubes," Phys. Fluids **36**(8), 081401 (2024).

Aziz, A. and El-Shaarawi, M. A. I., "Pressure loss in conical diffusers with large internal angles," J. Fluids Eng. **105**(2), 238–242 (1983).

Bird, R. B., Stewart, W. E., and Lightfoot, E. N., *Transport Phenomena*, 2nd ed. (John Wiley & Sons, 2007).

Crane Co., "Flow of fluids through valves, fittings & pipe, 80th anniversary edition," Technical Paper 410 (Chicago, 2022).

Davidson, L., "Hybrid LES/RANS for flows including separation: A new wall function using machine learning based on binary search trees," J. Turbul. **26**, 2476430 (2025).

Durst, F., Melling, A., and Whitelaw, J. H., *Principles and Practice of Laser-Doppler Anemometry* (Academic Press, 1993).

Escudier, M. P., Rosa, S., and Poole, R. J., "Asymmetry in transitional pipe flow of drag-reducing polymer solutions," J. Non-Newtonian Fluid Mech. **161**, 19–29 (2009).

Fox, R. W., McDonald, A. T., and Pritchard, P. J., *Introduction to Fluid Mechanics*, 8th ed. (Wiley, 2011).

Gao, T., Schmidt, H., Klein, M., Liang, J., Sun, M., Chen, C. P., and Guan, Q. D., "One-dimensional turbulence modeling of compressible flows: II. Full compressible modification and application to shock–turbulence interaction," Phys. Fluids **35**(3), 035116 (2023).

Gibson, A. H., *Hydraulics and Its Applications*, 4th ed. (Van Nostrand Co., Berlin, 1930).

Gooding, W. J., Fabian, J. C., and Key, N. L., "Laser doppler velocimetry characterization of unsteady vaned diffuser flow in a centrifugal compressor," J. Turbomach. **142**(4), 041001 (2020).

Han, Y., "A review on the application of hybrid RANS–LES methods in hydraulic machinery," Ocean Eng. **305**, 117943 (2024).

Hwang, P. W., Wu, J. H., and Chang, Y. J., "Optimization based on computational fluid dynamics and machine learning for the performance of diffuser-augmented wind turbines with inlet shrouds," Sustainability **16**(9), 3648 (2024).

Idelchik, I. E., *Handbook of Hydraulic Resistance*, 3rd ed. (Jaico Publishing House, 2005).

Massey, B. S., *Mechanics of Fluids*, 6th ed. (Chapman & Hall, London, 1989), p. 213.

Munson, B. R., Young, D. F., Okiishi, T. H., and Huebsch, W. W., *Fundamentals of Fluid Mechanics*, 7th ed. (Wiley, 2013).

Oliveira, P. J. and Pinho, F. T., "Pressure drop coefficient of laminar Newtonian flow in axisymmetric sudden expansions," Int. J. Heat Fluid Flow **18**, 518–529 (1997).

Oliveira, P., Pinho, F. T., and Schulte, A., "A general correlation for the local loss coefficient in Newtonianaxisymmetric sudden expansions," Int. J. Heat Fluid Flow **19**(6), 655–660 (1998).

Richardson, L. F. and Gaunt, J. A., "The deferred approach to the limit," Philos. Trans. R. Soc. A **226**, 299–349 (1927).

Rosa, S. and Pinho, F. T., "Pressure drop coefficient of laminar Newtonian flow in axisymmetric diffusers," Int. J. Heat Fluid Flow **27**, 319–328 (2006).

Runstadler, P. W. *et al.*, *Diffuser Data Book* (Creare Inc. Tech. Note 186, Hanover, 1975).

Shames, I. H., *Mechanics of Fluids*, 3rd ed. (McGraw-Hill International Editions, Berlin, 1992).

Shuiguang. T., Hang. Z., Huiqin. L., Yue. Y., Jinfu. L., and Feiyun. C., "Multi-objective optimization of multistage centrifugal pump based on surrogate model," J. Fluids Eng. **142**(1), 011101 (2020).

Suryanarayana, N. V. and Rao, Y. V. C., "Inlet velocity profiles and pressure drop in diffusers," Exp. Therm. Fluid Sci. **9**(1), 72–79 (1994).
Tanner, R. I., *Engineering Rheology* (Oxford University Press, NY, 2000).
Teklemariyem, D. A., "CFD parametric investigation of velocity increment induced by an empty diffuser: Optimization of geometric parameters for wind turbine applications," Heliyon **10**(4), e26782 (2024).
Tsui, Y.-Y. and Wang, C.-K., "Calculation of laminar separated flow in symmetric 2D diffusers," Trans. ASME **117**, 612–616 (1995).
White, F. M., *Viscous Fluid Flow*, 3rd ed. (McGraw-Hill, 2006).
White, F. M., *Fluid Mechanics*, 9th ed. (McGraw-Hill, New York, 2022).
Zeng, Y., Yao, Z., Tao, R., Liu, W., and Xiao, R., "Effects of lean mode of blade trailing edge on pressure fluctuation characteristics of a vertical centrifugal pump with vaned diffuser," J. Fluids Eng. **143**(11), 111201 (2021).